Fano line shapes in transmission spectra of silicon photonic crystal resonators

Karan K. Mehta, Jason S. Orcutt, and Rajeev J. Ram

Fano line shapes in transmission spectra of silicon photonic crystal resonators

Karan K. Mehta,[a] Jason S. Orcutt, and Rajeev J. Ram
Research Laboratory of Electronics, Massachusetts Institute of Technology, Cambridge, Massachusetts 02139, USA

Transmission measurements on symmetrically waveguide-loaded one-dimensional silicon photonic crystal microresonators are observed to exhibit Fano line shapes, which we find to be due to the interference between the resonant transmission and a leaky second-order quasi-transverse-electric mode partially guided through the photonic crystal. The line shape is tunable by varying the exciting fiber position, the material index, and via the cavity nonlinearity. This two-mode interference method applied to a one-dimensional silicon photonic crystal cavity represents a compact and tunable approach to obtaining such line shapes in integrated optical devices, with implications for efficient modulation of optical signals and nonlinear all-optical switching. © 2013 *American Institute of Physics*. [http://dx.doi.org/10.1063/1.4794064]

The interference between wave components transmitted through a discrete resonant state and a continuum channel gives rise to asymmetric spectra in a variety of settings, whether through quantum-mechanical or classical wave interference.[1,2] Classical electromagnetic interference of this kind in integrated optical resonators is of interest for a range of device applications.[3] In resonant optical modulators,[4] for example, with a given cavity quality factor (Q), asymmetric profiles can possess sharper features than Lorentzians and hence allow more energy efficient operation;[5] for the same reason, Fano line shapes can increase sensitivities of optical sensors based on resonance shifts.[6] Such features in coupled-resonator systems also play a basic role in the description of electromagnetically induced transparency (EIT)-like phenomena in dielectric and chip-based optical devices.[7–9]

In waveguide-coupled resonators, Fano and EIT-like interference can occur between two resonator modes coupled to the same feeding waveguide mode,[10–12] multiple modes of a bus waveguide coupled to the same resonator mode,[13–15] between separate resonators altogether,[8] or with separate waveguides for the continuum propagation.[16] Such interference has also been studied in silicon photonic crystal microcavities coupled to waveguides with partially reflecting elements before and after the cavity,[17,18] free-space scattering measurements on such cavities,[19,20] and claimed in photoluminescence measurements on microcavities employing one-dimensional ZnS:Mn/SiO$_2$ Bragg reflectors.[21]

In this work, the two interfering channels are the resonant transmission mediated by a quasi-one-dimensional (1D) photonic crystal cavity mode, and a second-order quasi-transverse electric (TE) mode of the bus waveguides that is leakily transmitted through the photonic crystal region (Fig. 1). The two modes have opposite symmetry about the propagation direction and are orthogonal, but interfere upon excitation of the same single-mode fiber (SMF) used to couple the transmitted light to the photodetector used in the measurement. Compared to previously studied geometries, here the use of a low mode-volume silicon microresonator, and a continuum state that is

transmitted through the cavity itself, allows for smaller footprint devices, active tuning and modulation via band-to-band absorption of a short wavelength pump, as well as low-power nonlinearities in the Fano effect[17,22] enabled by the interaction between the stored cavity energy and the silicon core.

The resonator used in these measurements was designed in a 1D crystal consisting of a linear array of holes in a waveguide. A hole tapering scheme[23] defines the cavity; with a fixed lattice constant of $a = 330$ nm, hole radii are tapered linearly from $r = 0.33a$ to $r = 0.28a$ over 10 lattice periods to either side of the cavity center, followed by 12 additional mirror holes with $r = 0.28a$, which controlled the coupling strength to the bus waveguides. The silicon core in the bus waveguides and the cavity has a width of 470 nm and a height of 225 nm. Fig. 1(a) shows the finite-difference time-domain (FDTD)-calculated electric field profile of the resonant mode[24] (the measured resonance at $\lambda = 1528.46$ nm is within 1.5% of the predicted frequency). The bus waveguide (without holes) is sufficiently wide to support a second-order quasi-TE mode, with odd symmetry. The patterned photonic crystal region does not support such a mode; however, near the resonant wavelength, about 40% of the power in the second-order bus mode is transmitted as a leaky wave through the photonic crystal region. A snapshot of the second-order mode propagating through the crystal, calculated by FDTD, is shown in Fig. 1(c).

The resonators in this work were fabricated with 193 nm immersion photolithography within a complementary metal-oxide-semiconductor (CMOS) process at Micron Technology, in the polycrystalline silicon (pSi) gate layer; as illustrated in Fig. 1(e), the pSi core in this process is clad in oxide as well as a silicon nitride (SiN) liner layer (which fills the holes in the cavity design), and the lower index contrast here as compared to other photonic crystal designs, as well as the intrinsic loss of the polycrystalline silicon waveguide[25] contributes to cavity loss. A future paper will discuss in more detail the characteristics of these resonators fabricated in this environment.[26]

Coupling of light into the device is achieved via a grating element,[27] which couples light from a nearly surface-normal
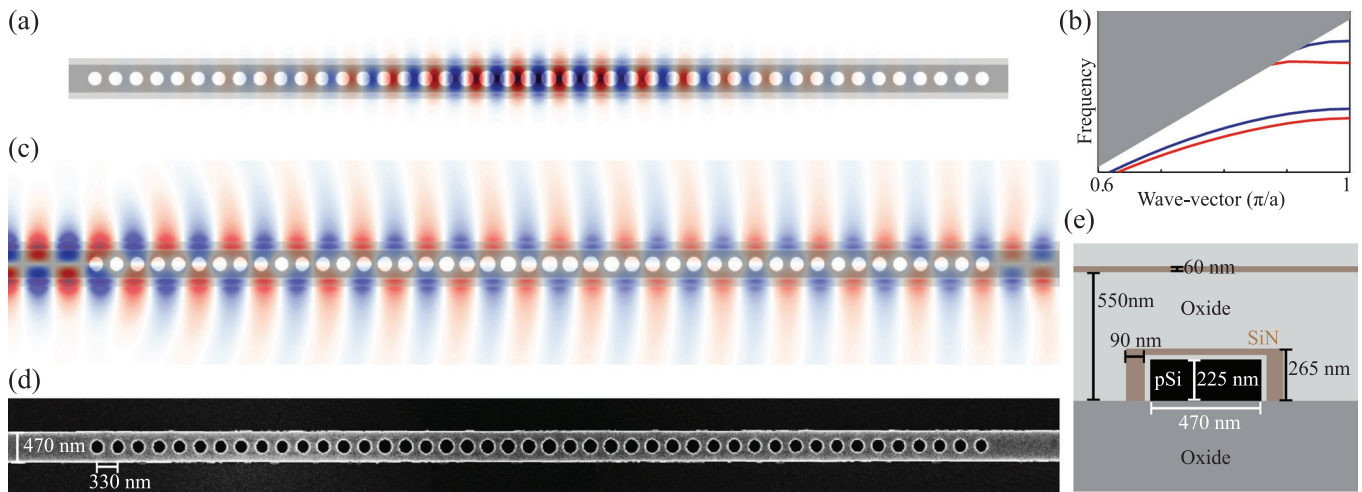
[a]Electronic mail: karanm@mit.edu.

FIG. 1. Schematic of cavity design and leaky mode; (a) resonant electric field, (b) schematic band diagram of 1D photonic crystal guided modes, with lowest two bands shown for waveguides with large (blue) and small (red) holes, and frequencies corresponding to leaky modes above the lightline shaded in gray; (c) FDTD calculation of second-order mode propagating through cavity; (d) dielectric environment around polycrystalline silicon (pSi) core in the CMOS process used, showing oxide cladding and SiN liner; and (e) SEM of the pSi of the fabricated cavity.

oriented cleaved SMF to the waveguide modes propagating in the plane of the chip, and a $200\,\mu$m-long taper which allows mode-size conversion (Fig. 2(a)). Transmission spectra are measured by sweeping a tunable laser across the resonant frequency and monitoring the outcoupled power. The grating couplers in the devices tested here are not optimal for the resonant wavelength of 1530 nm, and designed for a different dielectric environment than was present in these wafers; as a result, insertion loss through each of the two grating couplers is approximately 11 dB near resonance. Peak resonant transmission, determined by the ratio of the cavity decay rate into all modes and into the bus waveguide modes ($|T|^2 = Q_{\text{tot}}^2/Q_{\text{WG}}^2$) through the crystal,[28] is approximately -9 dB.

When the SMFs are nearly perfectly centered over the grating couplers along the direction labeled in Fig. 2(a), the odd second-order mode has vanishing overlap with the fundamental fiber mode and only the first-order waveguide mode is excited. Thus, very little interference with the

continuum occurs and the cavity transmission spectrum is expected to be Lorentzian; however, when both input and output fibers are displaced from the center (by a few μm in this case), the SMF modes now have nonzero overlap with the second-order mode, and some mixture of the two waveguide modes is coupled into and out of the device. The interference between the continuous and Lorentzian components, represented in the expression used to fit the measured transmission spectra,

$$|T(\omega)|^2 = \left| A_c e^{j\phi} + \frac{A_r \Gamma/2}{j(\omega - \omega_0) + \Gamma/2} \right|^2, \quad (1)$$

results in the Fano profiles.[20] In the expression above, the fields of the continuum states (amplitude A_c) and the Lorentzian resonance (with center frequency $\omega_0/2\pi$, peak transmitted amplitude A_r and total energy decay rate Γ) are summed with relative phase ϕ.
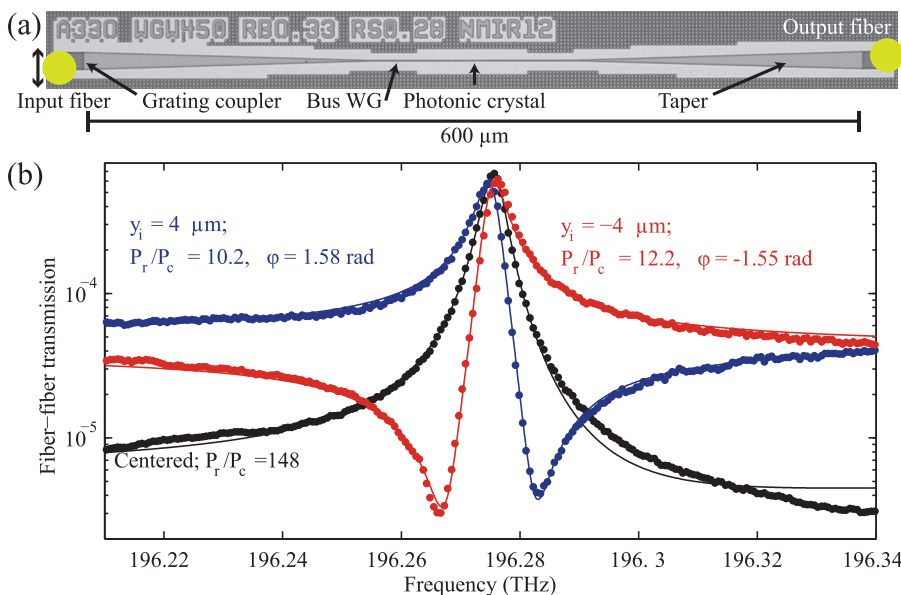

FIG. 2. (a) Optical micrograph of device tested, with grating couplers and surface normal oriented (i.e., out of page) fibers labeled. (b) Resonant measured transmission spectra (circles) and fits (lines), with input/output fibers centered (black); and with the output fiber slightly off-center by 2 μm and the input fiber at $y_i = \pm 4\,\mu$m (blue and red). The solid lines show fits to the data, all indicating a loaded Q of 45 000.

The role of the second-order mode in forming the continuum states could be confirmed by varying the positions of the input and output fibers in the direction shown in Fig. 2(a). Initially, both fibers are displaced from the center, so as to in- and out-couple some power in the second-order mode. If the input fiber had a displacement $+y_i$, moving it to $-y_i$ while keeping the output fiber at its original position should result in a $\Delta\phi = \pi$ between the two fiber positions, due to the odd symmetry of the second-order mode (and hence opposite overlaps between the second-order mode and the SMF mode at $\pm y_i$). Fig. 2 shows the results of measuring the transmission with the input SMF at -4 and $4\,\mu m$ from the center, with the output fiber held at the same position of μm from center. Transmission spectra obtained at these two input fiber positions reflect the opposite relative phase described above in the fact that the minimum of the asymmetric profiles occurs on opposite sides of the center wavelength for the different fiber positions. The profiles here show close agreement with fits to the profile in the equation above, which for the input fiber at -4 and $4\,\mu m$ gives $\phi = 1.58$ and -1.55 rad, corresponding to a 3.13 rad difference, very near the expected π. In the figure, each fit is labeled also with the ratio of the powers in the resonant mode to in the continuum $P_r/P_c = |A_r/A_c|^2$.

The observed variation of the line shape with fiber position gives evidence for the second-order mode forming the continuum. This mode can be launched from and interfered with the fundamental mode of a single mode waveguide using an integrated mode converter instead of coupling to SMFs, and a fully integrated device utilizing the various index tuning mechanisms studied to date in silicon (free carrier, depletion mode tuning, nonlinear optical tuning, for example) could benefit from the Fano profiles to achieve more energy efficient modulation of optical signals, regardless of the tuning mechanism.

As a demonstration of this, we measure the response of the cavity to 785 nm pump light shone directly onto the cavity through an additional third fiber; free carrier dispersion due to photoexcited electron-hole pairs tunes the resonance frequency. Approximately 2.5 mW from the pump laser was shone through a lensed fiber designed to create a spot size of $5\,\mu m$ diameter (at 1550 nm); together with the absorption coefficient of silicon, this results in an upper bound estimate of $30\,\mu W$ absorbed in the cavity, although in reality the coupled power was likely less since alignment was not optimal. The line shapes with the pump laser off (black) and on (red) are shown for the centered fibers and Lorentzian profile in Fig. 3(a), and for an offset alignment yielding a Fano profile in Fig. 3(b), with the same pump power applied to the cavity for both fiber alignments. In both cases, the resonance blueshifts, consistent with the effect of free carrier dispersion in silicon,[29] and the cavity Q decreases with the associated free carrier absorption, as is visible in the decreased peak transmission and broader line shape. For modulation, the optimal operation frequency of the signal light would be that corresponding to maximum contrast between points on the transmission spectra with pump on and off, which is exactly the resonance frequency here; whereas the Lorentzian feature gives approximately 10 dB of extinction for these tuning conditions, the Fano profile would give 17 dB. If the index were
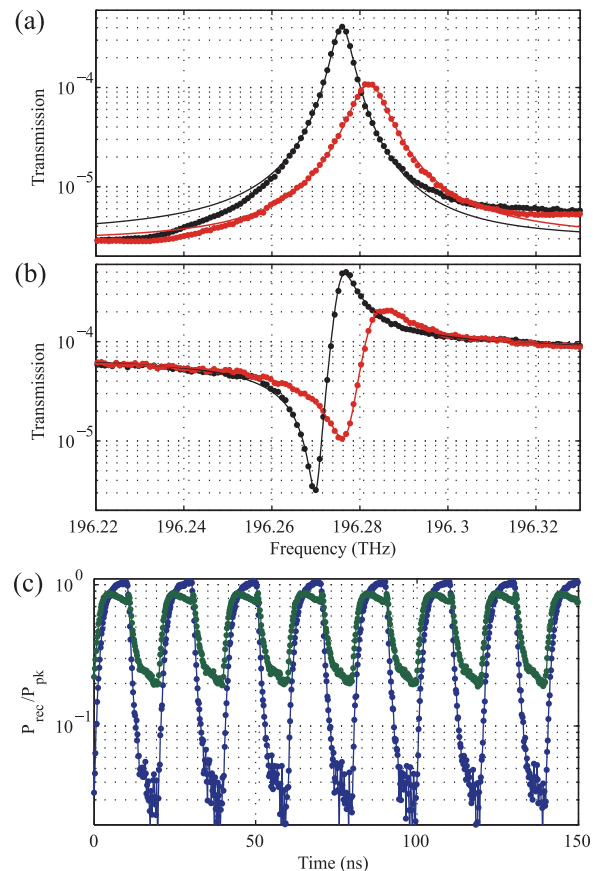

FIG. 3. Optical modulation via carrier excitation with 785 nm light; (a) tuning of Lorentzian feature, allowing a maximum of 10 dB extinction; (b) tuning of feature obtained with fibers off center and same 785 nm excitation, allowing 17 dB extinction; (c) 100 MB/s bit sequences applied to 785 nm laser, illustrating difference in extinction achievable with Fano (blue) and Lorentzian (green) profiles with the same modulation signal applied to the cavity in both cases.

tuned in a way that avoided the associated loss, the contrast would be significantly more pronounced, as a significant portion of the extinction in the Lorentzian case here is simply due to decreased peak transmission.

Fig. 3(c) illustrates the effect of these features on a bit sequence applied to the pump beam and transferred onto the initially continuous-wave signal beam propagating through the device. A 100 MB/s bit sequence of alternating 1s and 0s was applied by direct modulation to the pump laser, and the transmission of the infrared signal was measured for the cases of centered fiber alignment (green) and the Fano alignment (blue), clearly showing this contrast in extinctions. The bandwidth of this measurement is limited only by the direct modulation of the pump laser here; the cavity linewidth limit is approximately 5 GHz, and that from carrier recombination occurring on 100 ps timescales as expected in pSi of these dimensions would be 10 GHz. These measurements illustrate the utility of the second-order mode interference in increasing the achievable extinction under dynamic tuning, without increasing the tuning power or cavity Q.

We further note that the low mode volume of the 1D photonic crystal used in this work allows low-power nonlinear optical tuning, using the carriers excited by the photons in the cavity mode themselves; Fig. 4 shows single beam transmission spectra under three different incident powers, plotted as a function of detuning $\nu - \nu_0$ of the laser frequency ν from the
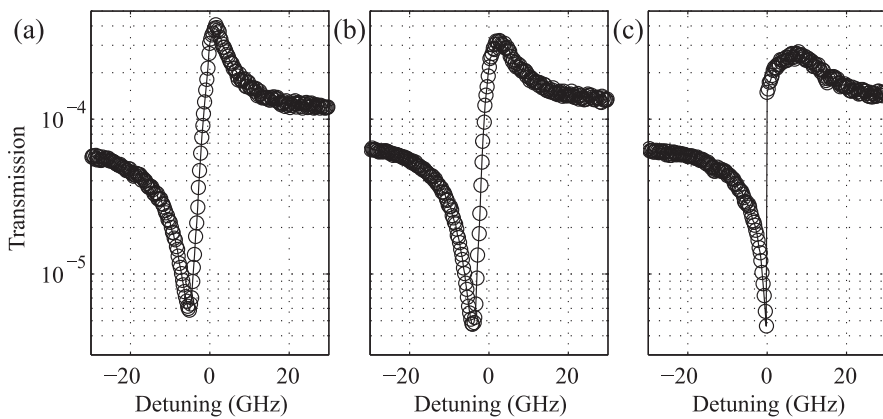
FIG. 4. Measured power-dependence of transmission spectra, with (a) 1.5 μW (b) 25 μW, (c) 85 μW coupled into the input bus waveguide. As the power is increased, the peak and minimum transmissions fall as the cavity Q and hence the power transmitted via the resonant channel decrease (b). Eventually bistability sets in, evident in the discontinuity in (c).

resonant ν_0. As the power increases, the photo-generated carriers contribute to loss, decreasing the Q and hence the resonantly transmitted power. The transmission in the continuum is comparatively weakly affected, however, altering the balance between the two transmission pathways and hence the maximum and minimum transmissions, as seen in Fig. 4(b). At powers larger than a few 10 s of μW in these devices, due to the heating of resonator by the stored energy and thermo-optic effect in silicon,[17,30,31] a bistability sets in, whose manifestation in the transmission spectrum discontinuity is particularly pronounced in the Fano line shape (Fig. 4(c)). The effect of Fano interference on bistable transmission has been studied, in detail, theoretically;[32,33] we leave study of such effects in this device to future work.

We have observed strongly tunable Fano profiles in the transmission spectra of 1D photonic crystal cavities, and found the interference between the resonant transmission and a leaky second-order mode of opposite symmetry responsible for the line shapes obtained. The increased modulation depth enabled by the sharp features in the Fano profile was demonstrated with all-optical modulation using a short-wavelength pump. Owing to both the small mode volume of the photonic crystal resonators used in this work and sharp features of the Fano profiles, future incorporation of integrated mode converters, along with electrical contacts to the resonators, will allow for efficient and compact electro-optic modulators. The realization here additionally allows the study of variations in the asymmetric line shapes and optical bistability arising from the intrinsic nonlinearity of the microcavity as a function of optical power in each of the two modes.

[1]U. Fano, Phys. Rev. **124**, 1866–1878 (1961).
[2]S. Fan, W. Suh, and J. D. Joannopoulos, J. Opt. Soc. Am. A **20**, 569–572 (2003).
[3]A. Miroshnichenko, S. Flach, and Y. Kivshar, Rev. Mod. Phys. **82**, 2257–2298 (2010).
[4]Q. Xu, B. Schmidt, S. Pradhan, and M. Lipson, Nature **435**, 325–327 (2005).
[5]M. A. Popovic, CLEO/IQEC, Baltimore, Maryland, May 2009, Paper CTuV6.
[6]C.-Y. Chao and L. J. Guo, Appl. Phys. Lett. **83**, 1527 (2003).
[7]S. Chu, B. Little, W. Pan, T. Kaneko, and Y. Kokubun, IEEE Photonics Technol. Lett. **11**, 1426–1428 (1999).
[8]Q. Xu, S. Sandhu, M. L. Povinelli, J. Shakya, S. Fan, and M. Lipson, Phys. Rev. Lett. **96**, 123901 (2006).
[9]W. Suh, Z. Wang, and S. Fan, IEEE J. Quantum Electron. **40**, 1511–1518 (2004).
[10]C.-H. Dong, C.-L. Zou, Y.-F. Xiao, J.-M. Cui, Z.-F. Han, and G.-C. Guo, J. Phys. B **42**, 215401 (2009).
[11]Y.-F. Xiao, L. He, J. Zhu, and L. Yang, Appl. Phys. Lett. **94**, 231115 (2009).
[12]B.-B. Li, Y.-F. Xiao, C.-L. Zou, Y.-C. Liu, X.-F. Jiang, Y.-L. Chen, Y. Li, and Q. Gong, Appl. Phys. Lett. **98**, 021116 (2011).
[13]A. Chiba, H. Fujiwara, J.-i. Hotta, S. Takeuchi, and K. Sasaki, Appl. Phys. Lett. **86**, 261106 (2005).
[14]A. C. Ruege and R. M. Reano, J. Lightwave Technol. **27**, 2035–2043 (2009).
[15]A. C. Ruege and R. M. Reano, J. Lightwave Technol. **28**, 2964–2968 (2010).
[16]S. Darmawan, Y. M. Landobasa, P. Dumon, R. Baets, and M. K. Chin, IEEE Photonics Technol. Lett. **20**, 9–11 (2008).
[17]X. Yang, C. Husko, C. W. Wong, M. Yu, and D.-L. Kwong, Appl. Phys. Lett. **91**, 051113 (2007).
[18]S. Fan, Appl. Phys. Lett. **80**, 908 (2002).
[19]M. Galli, S. L. Portalupi, M. Belotti, L. C. Andreani, L. O'Faolain, and T. F. Krauss, Appl. Phys. Lett. **94**, 071101 (2009).
[20]L. Babić and M. De Dood, Opt. Express **18**, 26569–26582 (2010).
[21]T. Baba, H. Makino, T. Mori, T. Hanada, T. Yao, and H. Lee, Appl. Phys. Lett. **87**, 171106 (2005).
[22]M. Kroner, A. O. Govorov, S. Remi, B. Biedermann, S. Seidl, A. Badolato, P. M. Petroff, W. Zhang, R. Barbour, B. D. Gerardot, R. J. Warburton, and K. Karrai, Nature **451**, 311–314 (2008).
[23]Q. Quan and M. Lončar, Opt. Express **19**, 18529–18542 (2011).
[24]A. F. Oskooi, D. Roundy, M. Ibanescu, P. Bermel, J. D. Joannopoulos, and S. G. Johnson, Comput. Phys. Commun. **181**, 687–702 (2010).
[25]J. S. Orcutt, S. D. Tang, S. Kramer, K. Mehta, H. Li, V. Stojanović, and R. J. Ram, Opt. Express **20**, 7243–7254 (2012).
[26]K. Mehta, J. Orcutt, O. Tehar-Zahav, Z. Sternberg, R. Bafrali, R. Meade, and R. Ram, (unpublished).
[27]D. Taillaert, P. Bienstman, and R. Baets, Opt. Lett. **29**, 2749–2751 (2004).
[28]Q. Quan, P. Deotare, and M. Loncar, Appl. Phys. Lett. **96**, 203102 (2010).
[29]R. Soref and B. Bennett, IEEE J. Quantum Electron. **23**, 123–129 (1987).
[30]P. Barclay, K. Srinivasan, and O. Painter, Opt. Express **13**, 801–820 (2005).
[31]L. Haret, T. Tanabe, E. Kuramochi, and M. Notomi, Opt. Express **17**, 21108–21117 (2009).
[32]V. Lousse and J. P. Vigneron, Phys. Rev. B **69**, 155106 (2004).
[33]A. Cowan and J. Young, Phys. Rev. E **68**, 046606 (2003).